now published
Eur. Phys. J. E, 25, 181-186 (2008) DOI: 10.1140/epje/i2007-10280-6

Biaxial liquid crystal elastomers: a lattice model

G. Skačej[1] and C. Zannoni[2]

[1] Oddelek za fiziko, Univerza v Ljubljani, Jadranska 19, SI-1000 Ljubljana, Slovenia

[2] Dipartimento di Chimica Fisica ed Inorganica and INSTM -CRIMSON-, Università di Bologna, Viale Risorgimento 4, I-40136 Bologna, Italy

Received: date / Revised version: date

Abstract. We present a lattice model for biaxial liquid crystal elastomers and perform large-scale Monte Carlo simulations in this model system. Uniaxial and biaxial orientational ordering clearly reflects in macroscopic spontaneous sample deformations. The simulation output is used to predict calorimetry data and deuterium magnetic resonance spectra.

PACS. 61.30.Vx Polymer liquid crystals – 61.30.Cz Molecular and microscopic models and theories of liquid crystal structure – 61.41.+e Polymers, elastomers, and plastics

1 Introduction

Crosslinked polymeric chains with embedded mesogenic units — liquid crystal elastomers — are functional rubber-like materials characterized by a pronounced coupling of mesogenic ordering and macroscopic elastic deformations. External stimuli such as temperature variation, ultra-violet irradiation, or an external electric field can induce changes in orientational mesogenic ordering and, consequently, in macroscopic sample shape [1]. In nematic elastomers, mesogenic units typically exhibit uniaxial ordering, while in the past a possibility of biaxial ordering in ordinary thermotropic nematics has been predicted theoretically [2], as well as from lattice [3] and off-lattice Monte Carlo (MC) simulations [4]. Recently, there have been a number of experimental observations of biaxial orientational order in thermotropic nematics, coming from x-ray [5], dynamic light scattering [6], and deuterium magnetic resonance (^{2}H NMR) studies [7,8]. Moreover, biaxial order has already been observed in nematic liquid-crystalline side-chain polymers [9,10].

These developments indicate that one can reasonably expect the synthesis of biaxial nematic elastomers capable of showing biaxial orientational order and, as a result, biaxial spontaneous deformations. Therefore, we believe

the time is appropriate to start analyzing theoretically some of properties expected from these novel materials and discussing the difference from uniaxial liquid crystals elastomers. In the present paper we thus propose a simple lattice model for biaxial liquid crystal elastomers, and perform large-scale MC simulations to predict the corresponding spontaneous deformations, as well as calorimetry data and ^{2}H NMR spectra. The proposed model is an evolution of our uniaxial lattice model for liquid crystal elastomers presented in Ref. [11].

2 Model

Following the lines of our earlier uniaxial study [11], the main elements of the model are i) rubber elasticity of the polymer network, ii) anisotropic interactions between biaxial mesogenic units, and iii) the strain-orientational coupling of the polymeric chains and mesogenic units. First, the sample is divided into N unit cells. The lattice points are taken to approximately correspond to crosslinks in the polymeric network, while the deformable lattice bonds substitute the connecting polymeric chains. In absence of elastic deformation and orientational order the unit cells are assumed to be simple cubic with side a.

Describing rubber elasticity we assume that the polymer chains are ideally flexible, and that they do not interact with each other and with the mesogenic units. Then, considering an affine elastic deformation λ that changes the unit cell sides from $\{a, a, a\}$ into $\{\lambda_x a, \lambda_y a, \lambda_z a\}$, we can write the rubber-elastic part of the pseudo-Hamiltonian as [11]

$$\mathcal{H}_e = N k_B T \alpha \left(\lambda_x^2 + \lambda_y^2 + \lambda_z^2\right). \tag{1}$$

Here $\alpha = 3a^2/2Mb^2$; M stands for the number of monomers between two crosslinks and b for the length of a single monomer. As elastomers are essentially incompressible, $\lambda_x\lambda_y\lambda_z = 1$.

The mesogenic material inside each unit cell is assumed to be close-packed and represented by a biaxial molecular cluster — "particle". For the ith unit cell its orientation is given by the orthonormal triad $\{\boldsymbol{s}_i, \boldsymbol{t}_i, \boldsymbol{u}_i\}$. Then, let $\boldsymbol{t}_i$ and $\boldsymbol{u}_i$ correspond to the short and long axis of the cluster, respectively. Assuming that the interaction between the molecular clusters is predominantly of dispersive origin (for a more general case see, e.g., [12]), the corresponding Hamiltonian reads [3]

$$\mathcal{H}_n = -\epsilon \sum_{\langle ij \rangle} \left\{ R^2_{00}(\omega_{ij}) + 2\nu \left[R^2_{02}(\omega_{ij}) + R^2_{20}(\omega_{ij}) \right] + 4\nu^2 R^2_{22}(\omega_{ij}) \right\} \tag{2}$$

where the sum runs over nearest neighbor cells i and j (assuming periodic boundary conditions), $\epsilon > 0$ is a constant, and ν is the molecular biaxiality parameter. ω_{ij} stands for the relative orientation of the neighboring particles i and j, defined by the three Euler angles, α_{ij}, β_{ij}, and γ_{ij}. R^2_{mn} are combinations of Wigner functions and are given by [13]

$$R^2_{00}(\omega_{ij}) = \frac{3}{2}\cos^2\beta_{ij} - \frac{1}{2}, \tag{3}$$

$$R^2_{02}(\omega_{ij}) = \sqrt{\frac{3}{8}}\sin^2\beta_{ij}\cos 2\gamma_{ij}, \tag{4}$$

$$R^2_{20}(\omega_{ij}) = \sqrt{\frac{3}{8}}\sin^2\beta_{ij}\cos 2\alpha_{ij}, \tag{5}$$

$$R^2_{22}(\omega_{ij}) = \frac{1}{4}(\cos^2\beta_{ij} + 1)\cos 2\alpha_{ij}\cos 2\gamma_{ij} - \frac{1}{2}\cos\beta_{ij}\sin 2\alpha_{ij}\sin 2\gamma_{ij}. \tag{6}$$

Alternatively, in terms of orthonormal triads the R^2_{mn}s become

$$R^2_{00}(\omega_{ij}) = \frac{3}{2}(\boldsymbol{u}_i \cdot \boldsymbol{u}_j)^2 - \frac{1}{2}, \tag{7}$$

$$R^2_{02}(\omega_{ij}) + R^2_{20}(\omega_{ij}) = \sqrt{\frac{3}{2}}\left[(\boldsymbol{t}_i \cdot \boldsymbol{t}_j)^2 - (\boldsymbol{s}_i \cdot \boldsymbol{s}_j)^2\right], \tag{8}$$

$$R^2_{22}(\omega_{ij}) = \frac{1}{4}\left[(\boldsymbol{t}_i \cdot \boldsymbol{t}_j)^2 + (\boldsymbol{s}_i \cdot \boldsymbol{s}_j)^2 - (\boldsymbol{t}_i \cdot \boldsymbol{s}_j)^2 - (\boldsymbol{s}_i \cdot \boldsymbol{t}_j)^2\right]. \tag{9}$$

For $\nu = 0$ $\mathcal{H}_n$ reduces to the Lebwohl-Lasher Hamiltonian for uniaxial particles [14], while $0 < \nu < 1/\sqrt{6}$ and $\nu > 1/\sqrt{6}$ simulate prolate and oblate biaxial particles, respectively. Depending on temperature and ν, an ensemble of biaxial particles can be found in the isotropic (I), nematic (N), or biaxial (B) phase. In the isotropic phase, no orientational order is present. In the nematic phase, for prolate particles their long axes $\boldsymbol{u}_i$ align, which is referred to as the "positive" nematic phase (N_+); analogously, oblate particles align along their short axes $\boldsymbol{t}_i$, forming the "negative" nematic phase (N_-). In the biaxial phase, all three particle axes ($\boldsymbol{s}_i$, $\boldsymbol{t}_i$, $\boldsymbol{u}_i$) are aligned [3].

Finally, orientational ordering couples to strain. In the uniaxial version of the model [11] this coupling is implemented via a Maier-Saupe-like mean field: mesogenic particles experience an aligning mechanical field along the fixed stretch direction, with a strain-dependent field strength. In the original Maier-Saupe theory for uniaxial ordinary nematics [15,16], the local aligning field strength is proportional to the degree of order of the surrounding nematic material. Analogously, here we adapt the mean-field treatment of orientational ordering in liquid crystals proposed by Straley for the biaxial case [2]. Then, denoting with ω_i the Euler angles for a relative orientation of ith particle and $\{\boldsymbol{x}, \boldsymbol{y}, \boldsymbol{z}\}$ — an orthonormal triad defining the principal axes of the biaxial sample deformation — one can write a coupling pseudo-Hamiltonian

$$\mathcal{H}_c = -\, k_B T \chi \sum_{i=1}^{N} \left[r^2_{00}(\lambda) R^2_{00}(\omega_i) + 2 r^2_{20}(\lambda) R^2_{20}(\omega_i)\right], \tag{10}$$

where χ is a coupling constant and $r^2_{mn}(\lambda)$ are the deformation-dependent quantities measuring the anisotropy of the polymer chain end-to-end tensor distribution (and, consequently, the strength of the mechanical field components). This distribution is represented by a biaxial ellipsoid $\mathcal{E}$ obtained by deforming a unit sphere at constant volume by the factors λ_x, λ_y, and λ_z along $\boldsymbol{x}$, $\boldsymbol{y}$, and $\boldsymbol{z}$, respectively. Denoting with θ and ϕ the polar and azimuthal

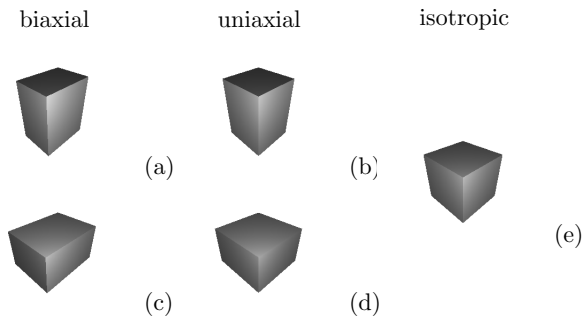

Fig. 1. Schematic depiction of sample shape (reflecting the symmetry of the polymer chain end-to-end tensor distribution) for different types of orientational ordering. In all cases the nematic director is vertical. (a-b) Positive materials with prolate mesogens, as well as negative materials with oblate mesogens. (c-d) Positive materials with oblate mesogens, or negative materials with prolate mesogenic units. (e) Undeformed sample, no orientational order.

angles measured with respect to $\boldsymbol{z}$ and $\boldsymbol{x}$, respectively, and with Ω the corresponding solid angle, the r^2_{mn}s are defined as

$$r^2_{00}(\lambda) = (4\pi)^{-1} \int_{\mathcal{E}(\lambda)} \left(\frac{3}{2} \cos^2\theta - \frac{1}{2} \right) \mathrm{d}\Omega, \qquad (11)$$

$$r^2_{20}(\lambda) = (4\pi)^{-1} \int_{\mathcal{E}(\lambda)} \sqrt{\frac{3}{8}} \sin^2\theta \cos 2\phi \; \mathrm{d}\Omega \qquad (12)$$

and are calculated numerically using the Simpson quadrature formula upon every deformation λ. In $\mathcal{H}_c$, $R^2_{mn}(\omega_i)$ can also be written as

$$R^2_{00}(\omega_i) = \frac{3}{2}(\boldsymbol{u}_i \cdot \boldsymbol{z})^2 - \frac{1}{2}, \qquad (13)$$

$$R^2_{20}(\omega_i) = \sqrt{\frac{3}{8}} \left[(\boldsymbol{u}_i \cdot \boldsymbol{x})^2 - (\boldsymbol{u}_i \cdot \boldsymbol{y})^2 \right]. \qquad (14)$$

Hence, having avoided terms depending on γ_i [i.e., $R^2_{02}(\omega_i)$ and $R^2_{22}(\omega_i)$] in $\mathcal{H}_c$ we actually assume that only the orientation of the particle long axis, $\boldsymbol{u}_i$, is actually coupled to the polymer network, while the other two axes, $\boldsymbol{s}_i$ and $\boldsymbol{t}_i$, are not.

The sign and the magnitude of the coupling parameter χ depend on the specific architecture of the elastomeric material [11]. Here, $\chi > 0$ describes "positive" materials in which mesogenic units align along the stretching direction, as in main-chain elastomers. Similarly, $\chi < 0$ can be attributed to "negative" materials where mesogens align perpendicular to the axis of stretching, like in some types of side-chain materials.

3 Monte Carlo simulations and observables

We have performed a large set of constant-force MC simulations to study the behavior of our model system. The MC evolution followed the standard Metropolis algorithm [17], with the total Hamiltonian given by $\mathcal{H} = \mathcal{H}_e + \mathcal{H}_n + \mathcal{H}_c$. Two types of MC trial moves were attempted: i) single particle reorientation and ii) sample resize moves. i) In generating single particle reorientations, both the rotation axis ($\boldsymbol{x}$, $\boldsymbol{y}$, or $\boldsymbol{z}$) and the rotation angle were chosen at random [18]. In every MC cycle each of the N particles was chosen once for a reorientation attempt, following a random sequence [19]. In case of acceptance, the corresponding triad $\{\boldsymbol{s}_i, \boldsymbol{t}_i, \boldsymbol{u}_i\}$ was updated. The acceptance of reorientation moves is driven by $\mathcal{H}_n$, $\mathcal{H}_c$, and temperature. ii) Every sample resize move consisted of generating a random variation of two simulation box sides, while the third box side was determined from the incompressibility constraint. The resize move affects $\mathcal{H}_e$ and $\mathcal{H}_c$. — The trial move amplitude for each move type was adjusted on the fly to maintain the corresponding acceptance ratio close to 50%, checking that evolution proceeds. Our system size was set to $N = 50^3$ unit cells. We have performed several heating and cooling MC run cascades. Every run was initialized with the equilibrated configuration obtained from the previous run at the nearest lower/higher temperature. Then, at least 70 MC kcycles were performed for equilibration and 66 kcycles for production.

In a heating/cooling temperature scan, structural transitions between the I, N_+, N_-, and B phases can be detected by calorimetry via anomalies in the heat capacity of the system, C_V. According to the fluctuation-response theorem, C_V can be related to fluctuations of internal energy U (calculated from $\mathcal{H}_n$) during the MC run. Then,

the corresponding dimensionless specific heat per particle is given by

$$c_V^* = \frac{C_V}{Nk_B} = \frac{\langle U^2\rangle - \langle U\rangle^2}{N(k_BT)^2}. \tag{15}$$

More direct information on biaxial orientational ordering can be extracted from thermodynamic averages $\langle R^2_{mn}\rangle$ [3]. Moreover, as orientational order couples to elastic deformation, the average simulation box sides, λ_x, λ_y, and λ_z, are also relevant observables.

Experimentally, biaxial orientational order in nematic polymers has been detected by ^{2}H NMR [9,10]. For this reason, we have used our simulation output to predict ^{2}H NMR spectra of biaxial elastomers. Deuterating mesogenic material yields an orientation-dependent quadrupolar frequency splitting ω_Q that, for the jth biaxial particle, is given by

$$\omega_Q^j = \pm\delta\omega_Q P_2(\mathbf{u}_j\cdot\mathbf{b}). \tag{16}$$

Here we have assumed that the electric field gradient (EFG) tensor of the carbon-deuteron bond is effectively uniaxial, with the symmetry axis of the tensor parallel to the long particle axis, $\mathbf{u}_i$. Further, $\mathbf{b}$ represents a unit vector parallel to the NMR spectrometer magnetic field and $\delta\omega_Q$ denotes a coupling constant [20]. Then, the spectra can be calculated by generating the free induction decay signal

$$G(t) = \left\langle \exp\left(i\int_0^t \omega_Q^j(t')\,dt' \right) \right\rangle_j, \tag{17}$$

where $\langle\cdots\rangle_j$ stands for ensemble averaging over particles, and Fourier-transforming it [21]. We believe that the MC reorientation moves reproduce the real mesogenic dynamics sufficiently well to produce reliable NMR spectra. — In each run, we have simultaneously calculated three spectra, with the spectrometer magnetic field directed along $\boldsymbol{x}$, $\boldsymbol{y}$, and $\boldsymbol{z}$, to easily detect any biaxiality in ordering. Translational diffusion was neglected. The duration of one NMR cycle, $2\pi/\delta\omega_Q$, was fixed to 1024 MC cycles. Finally, for smoothening, a convolution with a Lorentzian kernel of appropriate width was applied.

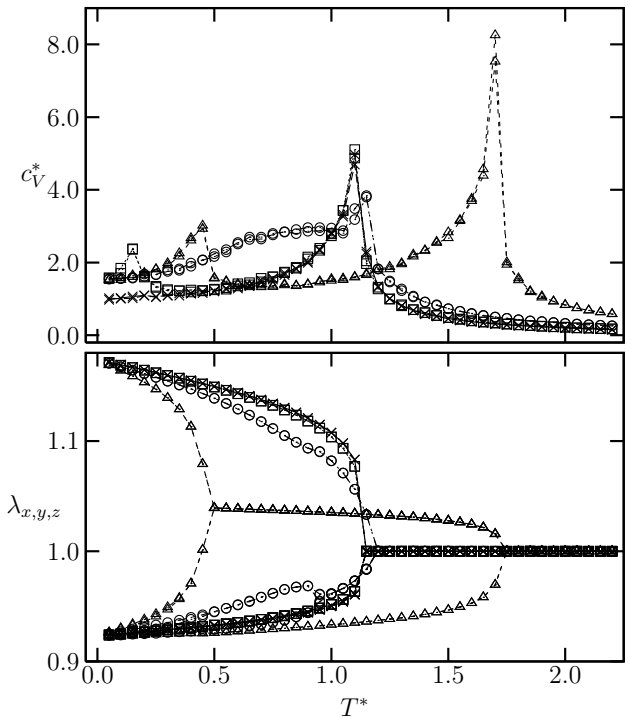

Fig. 2. Temperature dependence of specific heat (*top*) and average sample dimensions (*bottom*) for different values of the biaxiality parameter: $\nu = 0$ (×), $\nu = 0.2$ (□), $\nu = 1/\sqrt{6} \approx 0.4082$ (○), and $\nu = 0.6$ (△). Positive material, $\chi = 0.5$.

4 Results

Heating/cooling runs have been performed for positive and negative materials, as well as for different values of

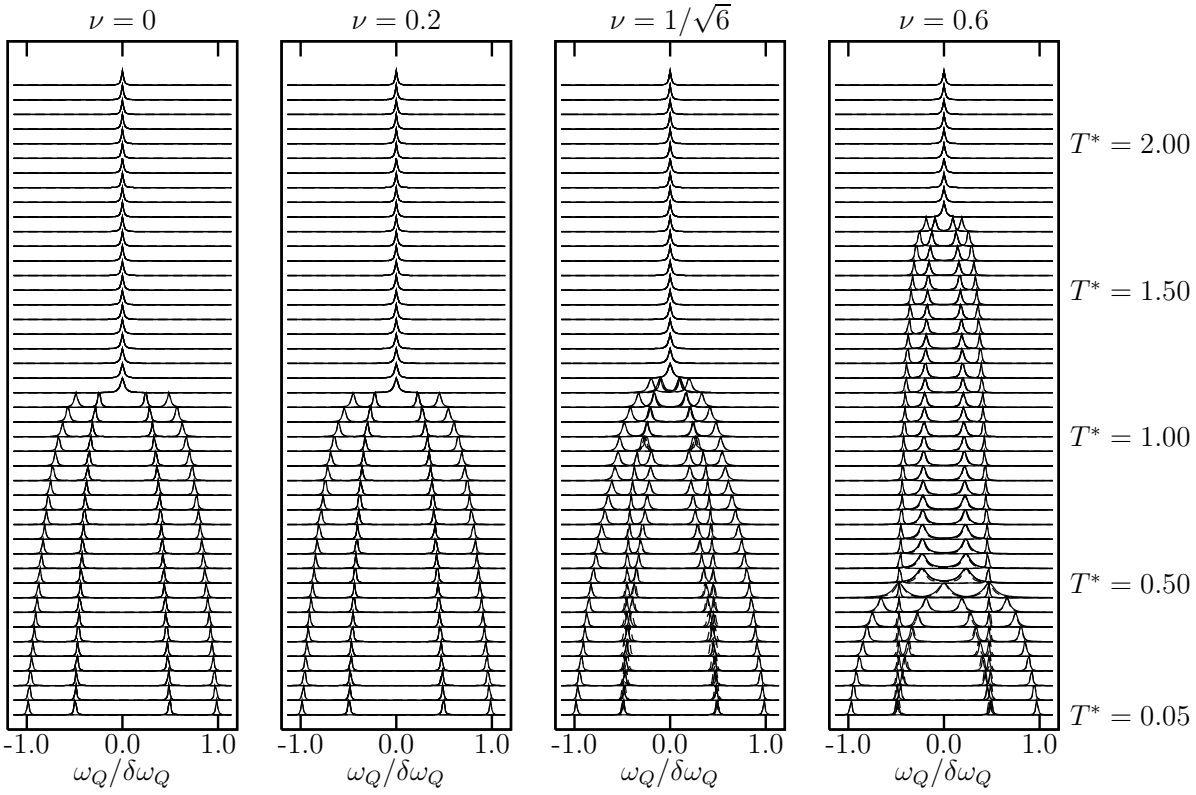

Fig. 3. Temperature dependence of ^{2}H NMR spectra for different values of ν. The spectrometer magnetic field was directed along $\boldsymbol{x}$, $\boldsymbol{y}$, and $\boldsymbol{z}$; the resulting spectral sets are superimposed. Positive material, $\chi = 0.5$. Note the absence of histeresis (at present resolution).

the biaxiality parameter ν. The parameter α [see Eq. (1)] that is related to the elastic modulus of the material was set to 0.3 as in Ref. [11]. Spontaneous deformation types, as observed during the runs, are shown schematically in Fig. 1.

Consider positive materials with $\chi = 0.5$ first. Setting $\nu = 0$, the pair potential for the interaction between mesogenic units, Eq. (2), becomes uniaxial as in Ref. [11]. On cooling from the isotropic phase the specific heat c_V^* (Fig. 2, *top*) peaks at $T^* = k_B T/\epsilon \approx 1.141 \pm 0.003$ [11], which is a signature of the weakly first-order isotropic-nematic (IN_+) phase transition. (A more detailed analysis [11] shows that the transition temperature is shifted to a slightly higher value in comparison with the ordinary liquid crystal, which is attributed to the order-stabilizing effect of the mechanical field.) The particle alignment is accompanied by a spontaneous deformation of about 8% along the director (Fig. 2, *bottom*) and a lateral contraction of about 4% to maintain volume constant. Cooling to even lower T^*, the spontaneous deformation increases together with the degree of nematic order. Fig. 3 shows the corresponding ^{2}H NMR spectra, with superimposed

curves for different spectrometer field orientations: $\mathbf{b}||\mathbf{x}, \mathbf{y}$, or $\mathbf{z}$, i.e., parallel or perpendicular to the nematic director $\mathbf{n}$. In the isotropic phase a single line at zero quadrupolar splitting is observed. In the nematic phase, however, a doublet appears at $\pm\Delta\omega$ and $\pm\Delta\omega/2$ for $\mathbf{b}||\mathbf{n}$ and $\mathbf{b} \perp \mathbf{n}$, respectively, where $\Delta\omega$ denotes the maximum frequency splitting observed for a given degree of order. The spectra for $\mathbf{b} \perp \mathbf{n}$ overlap as long as ordering is uniaxial. Decreasing T^*, $\Delta\omega$ — proportional to the degree of nematic ordering — increases.

Weakly biaxial prolate particles with $\nu = 0.2$ exhibit biaxial order, however only for $T^* < 0.2$. This can be deduced from a second peak in the temperature dependence of c_V^* reflecting the nematic-biaxial (N_+B) transition. The N_+B transition is of the second-order: the c_V^* peak is not as sharp as the one at $T^* \approx 1.15$ attributed to the IN_+ transition. For $\nu = 0.2$ the biaxiality is too weak to be detectable from asymmetries in lateral sample contraction or in ^{2}H NMR spectra for $\mathbf{b} \perp \mathbf{n}$.

In the ordinary liquid crystal, the stability temperature range of the biaxial phase is widest at the limit between prolate and oblate particles (for $\nu = 1/\sqrt{6} \approx 0.4082$) where there is a direct second-order isotropic-biaxial (IB) transition [3] at the Landau point. Performing a cooling run with our model elastomer for $\nu = 1/\sqrt{6} \approx 0.4082$ this direct IB transition splits into a pair of near transitions: IN_+ at $T^* \approx 1.17 \pm 0.01$ and N_+B at $T^* \approx 0.96 \pm 0.01$. The latter transition can be reliably detected only from the asymmetry in lateral sample dimensions as the corresponding c_V^* peak is extremely broad. The biaxial asymmetry is now clearly visible also from ^{2}H NMR spectra: the two $\mathbf{b} \perp \mathbf{n}$ spectral sets do not overlap any longer, except in the narrow temperature window where ordering is uniaxial.

Results from more detailed temperature scans are summarized in the phase diagram shown in Fig. 4. From the diagram one can deduce that the Landau point has actually moved to $\nu \approx 0.414 \pm 0.001$, i.e., that the stability range of the N_+ phase formed by prolate (rod-like) mesogenic particles has slightly increased at the expense of the N_- phase formed by oblate (plate-like) particles. This is another consequence of the mechanical field presence: as in our model the particle alignment couples to strain exclusively via the orientation of the particle long axis $\mathbf{u}_i$ — see the expression for $\mathcal{H}_c$ — the mechanical field stabilizes the alignment of $\mathbf{u}_i$, rather than that of the short axes $\mathbf{t}_i$. Hence, the N_+ phase becomes favored over N_-.

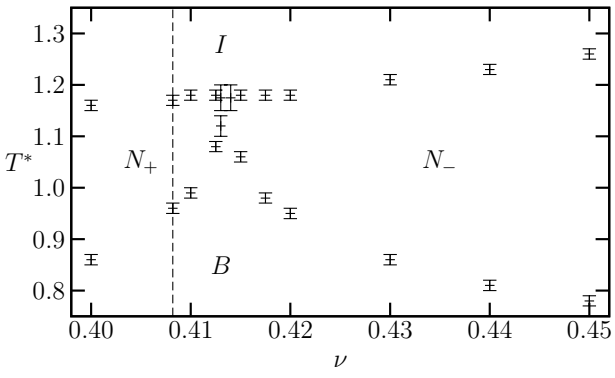

Fig. 4. Orientational phase diagram of a biaxial elastomer (positive material, $\chi = 0.5$). Note the shift of the Landau point from $\nu = 1/\sqrt{6} \approx 0.4082$ (dashed line) to a slightly higher value.

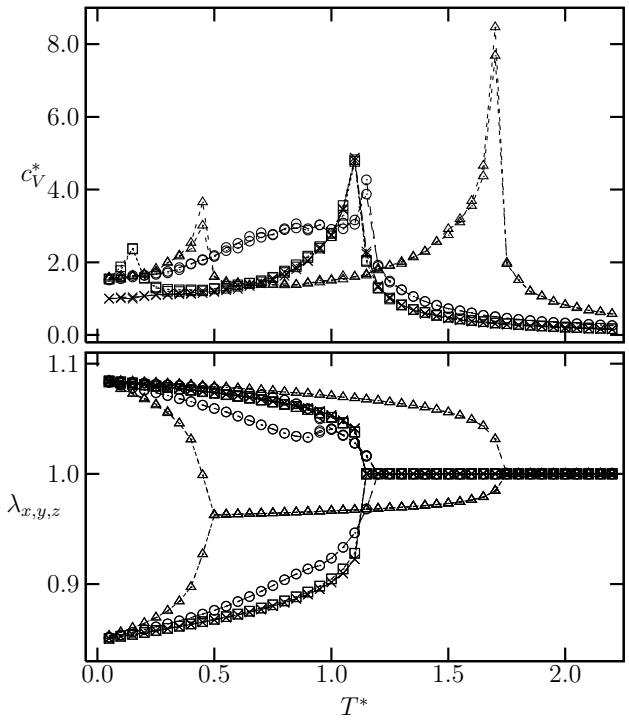

Fig. 5. Same as Fig. 2 (including key), yet for a negative material with $\chi = -0.5$. While the c_V^* temperature dependences (*top*) are almost identical to those calculated for the positive material, the sample deformations λ_x, λ_y, and λ_z (*bottom*) are quite different.

For oblate particles the isotropic phase on cooling transforms into the negative nematic phase, where the short particle axes are aligned. While for prolate particles the IN_+ transition temperature was essentially ν-independent, this is no longer the case for oblate particles. For $\nu = 0.6$ the IN_- transition takes place at $T^* \approx 1.75$, while the N_-B transition can be observed at $T^* \approx 0.50$; see Fig. 2. In the N_- phase the sample contracts along the director and expands laterally. The degeneracy of the lateral sample sides is lifted once in the biaxial phase. The ^{2}H NMR spectra show two pairs of peaks: one at $\pm\Delta\omega/2$ and one at $\pm\Delta\omega/4$, corresponding to $\mathbf{b}||\mathbf{n}$ and $\mathbf{b} \perp \mathbf{n}$, respectively. (Recall that $\mathbf{n}$ here is assigned to the average orientation of the short molecular axes $\mathbf{t}_i$ and that the EFG tensor principal axis is directed along the long axes $\mathbf{u}_i$ that are moving fast on the ^{2}H NMR time scale.) Again, the peaks at $\pm\Delta\omega/4$ split once biaxial order is obtained.

We have also performed a sequence of heating runs that are also shown in all plots. Note that the curves essentially overlap and hysteresis in all cases (at current precision) is negligible.

Let us also comment on negative (e.g., end-on side chain) materials, taking $\chi = -0.5$. The orientational ordering behavior (and, consequently, the resulting ^{2}H NMR spectra) is essentially the same as for positive materials. The main difference appears in average sample dimensions: for example, in the N_+ phase a positive material expands along $\mathbf{n}$, while a negative material contracts (Fig. 5). In the N_- phase a positive material contracts along $\mathbf{n}$, and vice versa for a negative material. Again, in the B phase, the symmetry of the two lateral components (perpendicular to $\mathbf{n}$) is broken. See also Fig. 1.

5 Conclusions

We have developed a coarse-grained lattice model for biaxial liquid crystal elastomers, treating elastomers with both prolate and oblate mesogenic units, as well as positive and negative materials in terms of strain-alignment coupling. Our model elastomer can be found in the biaxial, uniaxial nematic (either positive or negative), and

isotropic phase, which clearly reflects in predicted average sample shape, as well as in simulated ^{2}H NMR spectra. The stability range of rod-like (prolate) nematic ordering is sligthly increased at the expense of plate-like (oblate) ordering, which implies a shift of the Landau point to a somewhat higher molecular biaxiality value in comparison with an ordinary biaxial nematic.

This work was carried out within the FULCE (Functional Liquid Crystalline Elastomers) Research Training Network funded by the European Union. Further financial support from PRIN #2005035119 and the Slovene-Italian bilateral project BI-IT/06-09-F9 (Mrežne simulacije tekočekristalnih elastomerov/Simulazioni su reticolo di elastomeri liquido cristallini) is acknowledged.

References

1. M. Warner and E. M. Terentjev, *Liquid Crystal Elastomers* (Oxford University Press, Oxford 2003).
2. J. P. Straley, Phys. Rev. A **10**, (1974) 1881.
3. F. Biscarini, C. Chiccoli, P. Pasini, F. Semeria, and C. Zannoni, Phys. Rev. Lett. **75**, (1995) 1803.
4. R. Berardi and C. Zannoni, J. Chem. Phys. **113**, (2000) 5971.
5. B. R. Acharya, A. Primak, and S. Kumar, Phys. Rev. Lett. **92**, (2004) 145506.
6. K. Neupane, S. W. Kang, S. Sharma, D. Carney, T. Meyer, G. H. Mehl, D. W. Allender, S. Kumar, and S. Sprunt, Phys. Rev. Lett. **97**, (2006) 207802.
7. L. A. Madsen, T. J. Dingemans, M. Nakata, and E. T. Samulski, Phys. Rev. Lett. **92**, (2004) 145505.
8. J. L. Figueirinhas, C. Cruz, D. Filip, G. Feio, A. C. Ribeiro, Y. Frère, T. Meyer, and G. H. Mehl, Phys. Rev. Lett. **94**, (2005) 107802.
9. K. Severing and K. Saalwächter, Phys. Rev. Lett. **92**, (2004) 125501.
10. K. Severing, E. Stibal-Fischer, A. Hasenhindl, H. Finkelmann, and K. Saalwächter, J. Chem. Phys. B **110**, (2006) 15680.
11. P. Pasini, G. Skačej, and C. Zannoni, Chem. Phys. Lett. **413**, (2005) 463.
12. A. M. Sonnet, E. G. Virga, and G. E. Durand, Phys. Rev. E **67**, (2003) 061701.
13. M. E. Rose, *Elementary Theory of Angular Momentum* (Wiley, New York 1957).
14. P. A. Lebwohl and G. Lasher, Phys. Rev. A **6**, (1972) 426.
15. W. Maier and A. Saupe, Z. Naturforsch. A **14**, (1959) 882.
16. W. Maier and A. Saupe, Z. Naturforsch. A **15**, (1960) 287.
17. N. Metropolis, A. W. Rosenbluth, M. N. Rosenbluth, A. H. Teller, and E. Teller, J. Chem. Phys. **21**, (1953) 1087.
18. J. A. Barker and R. O. Watts, Chem. Phys. Lett. **3**, (1969) 144.
19. U. Fabbri and C. Zannoni, Mol. Phys. **58**, (1986) 763.
20. R. Y. Dong, *Nuclear Magnetic Resonance of Liquid Crystals* (Springer Verlag, New York 1994).
21. C. Chiccoli, P. Pasini, G. Skačej, S. Žumer, and C. Zannoni, Phys. Rev. E **60**, (1999) 4219.